

## Measurement of impurity profile modifications with a modulated diagnostic beam on Tore Supra

Hess W.R., DeMichelis C., Hogan J.<sup>+</sup>, Farjon J.L., Druetta M.\*<sup>,</sup> Bush Ch.<sup>+</sup>

Association EUR-CEA, CEN-Cadarache, F-13108 St-Paul-lez-Durance, France

\*Université Jean Monnet, TSI-UMR CNRS 5516, F-42023 Saint Etienne Cedex 2, France

<sup>+</sup> Fusion Energy Division, Oak Ridge National Laboratory, Oakridge, TN 37830, USA

A dedicated diagnostic beam of moderate power (45kW) is used on Tore Supra for charge exchange recombination spectroscopy (CXRS). Even in ohmic heated discharges no perturbation of the plasma due to the power deposition of the beam is expected. The neutral beam (45kV, 1A @ plasma edge, hydrogen) is modulated with equally spaced pulses of 10 to 100ms. Synchronisation of two

detection systems (grating spectrometer with CCD camera and fast PM filter spectrometer) shows the possibility of obtaining, by subtraction of the background signal, virtually pure charge exchange spectra (CXRS) for both intrinsic impurities (carbon) and injected impurities (neon). Fig:1 shows the CVI CXRS signal observed on the central viewing line with the filter spectrometer (time resolution 4ms). The CX signal is easily subtracted from the plasma edge emission.

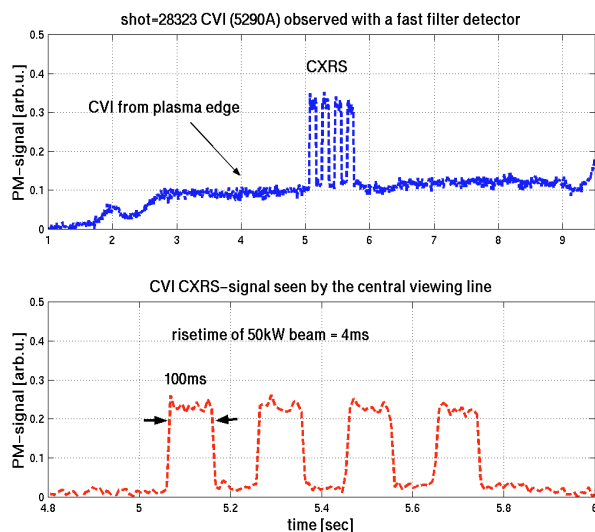


Fig.:1 CVI signal observed with fast filter spectrometer

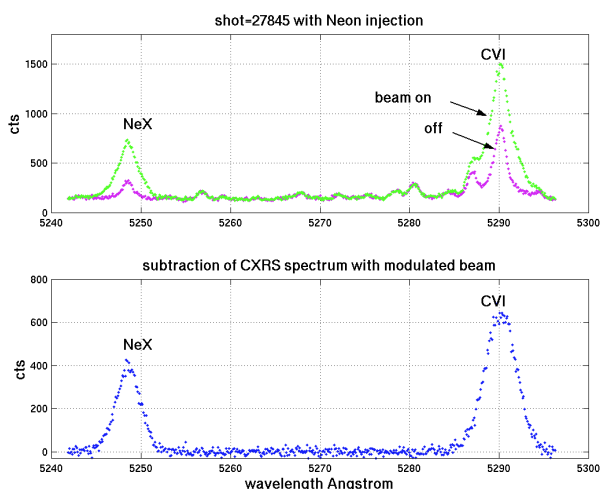


Fig.:2 NeX and CVI visible spectrum w/o subtraction

Fig.2 shows the Neon and Carbon spectrum and the extracted CX-spectrum at 5.9s of an Ergodic Divertor shot with ICRH-heating. At 3.5s Neon is puffed into the plasma. The diagnostic beam is fired at 6.9s (ICRH=0.8MW) where the Ti and impurity profiles are measured. The vertical beam (45kV, 1A) is seen by a fan of 8 viewing lines within a vertical plane. A grazing incidence soft X-ray spectrometer views the neutral beam at the plasma centre.

**Impurity density in the plasma core and edge region:** The CX-signal for the ground state transition (Lyman- $\alpha$ ) of NeX, OVII and CVI and the emission due to electron excitation at the plasma edge are used to calculate the impurity ratio in the plasma centre and in the edge region (fig:3). Only the relative CX-cross-sections (ADAS-data base) and calibration factors are necessary for the core.

A 1D impurity transport code is used (see below) to determine the position of each ion emission layer. Knowing the electron density and temperature at the emission location and thus the photon emissivity coefficients, the impurity density for the main three species in the core and edge region can be deduced. The ratio core/edge is an important value for the evaluation of the ED purification action [Ref.:].

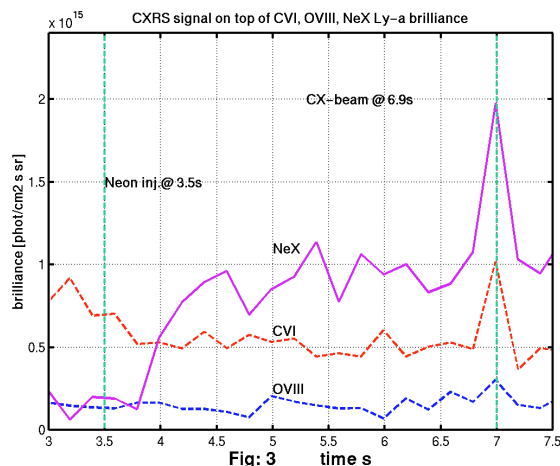


Fig.:3 XUV signal of the main impurities with the core CX signal when the diagnostic beam is fired

**Ion temperature gradient and poloidal rotation profiles:**

A series of deuterium discharges with ICRH heating is analysed; the diagnostic beam was fired before and during the RF pulse. As the ICRH-power reaches its plateau value of 4.3MW (H-minority heating with central power deposition) the gradient of the Ti-profile in the plasma centre  $\rho \leq 0.4$  increases from 2.8 to 7.1 keV/m (fig:4). At the same time a strong change of the poloidal rotation velocity  $v_\theta$  is observed (fig.:5). Within the plasma core  $\rho \leq 0.4$  the change of  $v_\theta$  can be as high as 3.5 km/s. Comparing the spectral position of the CX-line to the unshifted position of the CVI line of the cold, recombining plasma a red-shift is obtained which results in a rotation in the electron diamagnetic drift direction.

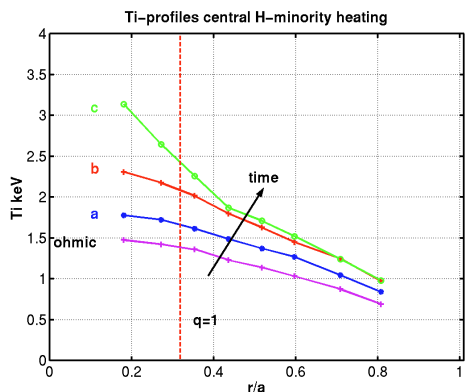


Fig.: 4 change of Ti gradient during ICRH

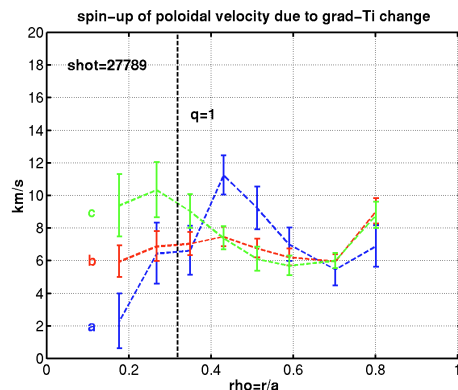


Fig.: 5 poloidal rotation profile change

The increase of the clockwise rotation could be due to transport changes induced by ICRH. Simulations with the NEOCLASS code show poloidal rotation velocities one order of magnitude lower ( $v_\theta < 1 \text{ km/s}$  for C, Ne) than the measured values. An estimation of the neoclassical  $\Delta v_\theta$  due to the grad-Ti change yields  $\Delta v_\theta = 0.3 \text{ km/s}$ , also 10x smaller than the observed value. Unfortunately the time evolution of  $v_\theta$  could not be followed because of the short duration of the diagnostic beam. Atomic physics effects on the shape of the CX line as discussed in Ref:1 are not included. They do not affect the shape and the differential values of the poloidal rotation profile but they might affect the absolute value because of high beam-fractions at low energy.

### Impurity transport and radiation properties for ergodic divertor plasma:

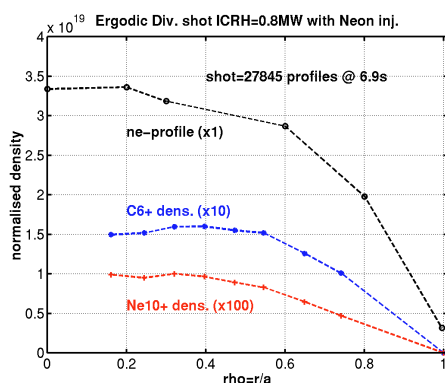


Fig.: 6  $C^{6+}$ ,  $Ne^{10+}$  and  $n_e$  profiles

A coherent picture of impurity transport and radiation properties of plasmas with the TS-Ergodic Divertor can be drawn using the measured impurity profiles together with a 1D transport code for the confined region and a 3D code (BBQ, Ref.2) for the edge (divertor) region. The shape of  $D, v_d$  (respectively the diffusion coefficient and inward velocity of the impurity ion of interest) is fixed by the measured  $C^{6+}$ ,  $Ne^{10+}$  profiles (fig:6). A clear  $Z$  dependence of the core impurity transport as discussed in Ref:3 is not observed. There is only a slight difference between  $Z=6+$  and  $10+$ , so that the  $C^{6+}(D, v_d)$  is also used for O and Ne.

Absolute impurity concentrations are calculated using Zeff-bremsstrahlung, absolute soft X-ray brilliances and spectroscopic beam-power measurements. As stated above, the C/O ratio, which is 6/1 in the plasma centre, is obtained via the Lyman- $\alpha$  CX-signal.

### Transition between the 1D and ergodic divertor (ED) region and radiation pattern:

$D$  shows a step in the ED region ( $r/a > 0.8$ ), typically a factor of 3.5 higher than the core value.

Three different zones are considered in the following:

- (1) the core, extending from  $r/a=0$  up to  $r/a \sim 0.8$  (LCFS)
- (2) the ED zone between  $r/a \sim 0.8$  and the ED-SOL at  $r/a=0.99$  and
- (3) the zone close to the divertor panels with their neutraliser plates.

Zone (3) is modelled with the 3D (BBQ) code which includes the 'fine structure' of the ergodic region. For the intermediate zone (2) radially averaged 1-D values ( $D, v_d$ ) [5] are used in the 1D code. The 'internal' 3D ergodic zone is thus modelled in a similar way as the treatment of ELM- (or sawtooth-) affected regions of poloidal divertor plasmas.

Fig:7 shows the details of the emission profiles obtained with the 1D-transport code. As already stated, enhanced  $D, v_d$  values are used for  $r/a > 0.8$ .

Clearly, most of the radiated power of C, O comes from the intermediate zone (2) whereas the NeX, NeIX radiation issues from zone (1) as confirmed by a completely symmetric radiation belt observed by the bolometers.

Using the 3-zone scheme, the calculated, total radiated power  $P_{\text{tot}}=1.74\text{MW}$  is distributed in the following way:

Only a small fraction, about 10%, is attributed to zone (3). The major contribution, 1.3MW, comes from (2) and 17%, mostly due to Neon, from (1). The total radiated power measured by the bolometer, which does not see the ED panels, is 1.4MW.

### Outlook and Conclusions:

A series of steps can be foreseen to improve the correspondence. First, replace the neutral particle fluxes in the ‘averaged’ 1D code with the more realistic case of charged particle influxes. Then, extend the self-consistently modelled 3D region inward, by using the ED magnetic field structure in BBQ. In this way the CXS profiles, which determine the profile from  $r/a=0$  outwards up to the ED region, can be joined with 3D simulations of the ED region to fix the inward fluxes for the 1D calculations using the 1D ‘divertor-averaged’  $D$ ,  $v_d$  values in the ergodic zone.

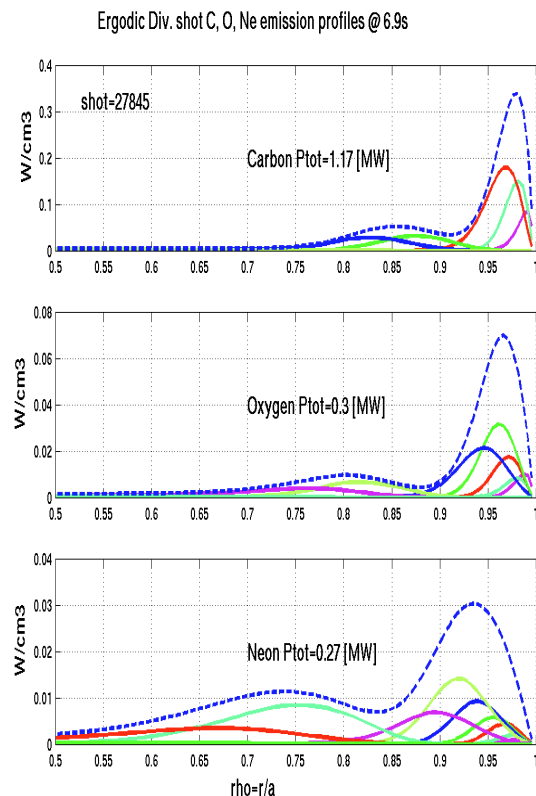


Fig.:7 Emission profiles of C,O,Ne

### References:

- [1] E.J.Synakowski et al., PPPL Princeton, USA; 4<sup>th</sup> Int. IEA Workshop on Helium Transport, Jekyll Island, USA, (1999)
- [2] J.Hogan et al., Proceedings of the 16<sup>th</sup> IAEA Int. Conf. on Plasma Phys. and Contr. Fus. Research, Vol.2, Montreal (1996) 1
- [3] R.Dux et al., Nuclear Fusion, Vol.39, n°11 (1999) 1509
- [4] R.Guirlet et al., presented at 14<sup>th</sup> Int. Conf. on Plasma Wall Inter., Rosenheim (2000)
- [5] M.Z.Tokar, Physics of Plasma, vol.6, n°7 (1999) 2808